

# Modeling and simulation of the horizontal component of the magnetic field by fractional stochastic differential equations in conjunction with empirical mode decomposition

Zu-Guo Yu<sup>1,2</sup>, Vo Anh<sup>1,3\*</sup>, Yang Wang<sup>4</sup> and Dong Mao<sup>4</sup>

<sup>1</sup>School of Mathematical Sciences, Queensland University of Technology,  
GPO Box 2434, Brisbane, Q4001, Australia.

<sup>2</sup>School of Mathematics and Computational Science, Xiangtan University, Hunan 411105, China.

<sup>3</sup>Florida Space Institute, University of Central Florida, Orlando, Florida 32816-2370, U.S.A.

<sup>4</sup>Department of Mathematics, Michigan State University, East Lansing, MI 48824-1027, USA.

## Abstract

In this paper, we investigate the scaling behaviour of ground magnetometer measurements based on the data at 22 stations of the INTERMAGNET. This behaviour would be useful in identifying the source which causes the fluctuations in some regions of the magnetosphere.

The time series of the  $B_x$  component at each station is modeled as the solution of a fractional stochastic differential equation. A method to estimate the parameters based on observed data and to simulate the model is given. The degree of fractional differentiation and the  $\alpha$ -stability exponent of the noise process driving the equation are employed to cluster the stations. The  $B_x$  time series possess pronounced local trends, which must be removed before clustering can be performed. This trend removal is carried out via an empirical mode decomposition. A by-product is an efficient method to simulate  $B_x$  time series via empirical mode decomposition and fractional stochastic differential equations.

The numerical results indicate the existence of two distinct regions of scaling: one in the low latitudes near the equator similar to that of the  $D_{st}$ , and the other above latitude  $60^\circ N$  consistent with the AE. These scalings are characteristic of each region, which maps into the magnetospheric region related to the solar wind and the inner magnetosphere respectively.

## 1 Introduction

Earlier works by Consolini *et al.* (1996), Uritsky and Pudovkin (1998), Chapman *et al.* (1998), Chang (1999) in modeling the magnetosphere in the framework of self-organized criticality (SOC) motivated many recent studies on stochastic properties of the magnetosphere and related geomagnetic indices. In an SOC model, simple local interactions produce complex global signatures of a system. These signatures may appear in the form of power-law scaling in the probability distributions or in the power spectra. For example, Freeman and Watkins (2002) noted that the probability

---

\*Corresponding author, email: v.anh@qut.edu.au

distribution of the time for which the AE index exceeds a given threshold follows a power law distribution. In investigations of the spatial structure of the aurora using ultraviolet images from NASA’s polar spacecraft, Lui *et al.* (2000) found a power law relationship between the number of bright spots and their area, and Uritsky *et al.* (2002) found power laws for the probability distribution of bright spot lifetime and maximum dissipated energy. An explanation of some aspects of these power laws was given in Klimas *et al.* (2004) in an SOC-like reconnection-based model. A review on the scaling in the AE and other geomagnetic indices was provided in Watkins *et al.* (2005).

Pulkkinen *et al.* (2006) developed an Itô-type stochastic model for the AE index to investigate the role of stochastic fluctuations in the global dynamics of the magnetosphere-ionosphere system. Anh *et al.* (2008) provided a fractional stochastic differential equation for the hourly AE index for the period 1978-1987. The memory of the AE time series is represented by a fractional derivative, while its heavy-tailed behavior is modeled by a Lévy noise with inverse Gaussian marginal distribution. The equation has the form of the classical Stokes-Boussinesq-Basset equation of motion for a spherical particle in a fluid with retarded viscosity. The fractional order of the equation conforms with the previous finding that the fluctuations of the magnetosphere-ionosphere system as seen in the AE reflect the fluctuations in the solar wind: They both possess the same extent of fractional differentiation.

These high-latitude fluctuations, which typically occur above geomagnetic latitude  $60^\circ N$  as manifested in the AE index, reflect solar wind conditions. On the other hand, low-latitude geomagnetic fluctuations, as seen in the  $D_{st}$  index, are believed to connect directly to the inner magnetosphere. Wanliss and Reynolds (2003) suggested that “examination of low-latitude ground magnetometer signals can provide clues as to whether the magnetosphere is inherently self-organized”. Wanliss and Reynolds (2003) analyzed hourly magnetometer measurements of total magnetic field strength from 6 stations at low latitudes over the period 13-18 January 1993. Using spectral analysis and rescaled range analysis, they found, at this hourly resolution, a relative increase of the Hurst exponent with latitude, and suggested that the result “may help quantify the dynamics of the inner magnetosphere itself without the direct presence of the solar wind driver”. With regard to the  $D_{st}$  itself, Wanliss (2004, 2005) and Wanliss and Dobias (2007) found that the  $D_{st}$  index exhibits a power-law spectrum with the Hurst parameter varying over different segments of the time series. This behavior indicates that  $D_{st}$  is a multifractional process.

Fractal and multifractal approaches have been quite successful in extracting salient features of physical processes responsible for the near-Earth magnetospheric phenomena (Lui, 2002). Heavy-tailed Lévy-type behavior has been observed in the interplanetary medium and the magnetosphere (Burlaga, 1991, 2001; Burlaga *et al.*, 2003; Kabin and Papitashvili, 1998; Lui *et al.*, 2000, 2003). A method to describe the multiple scaling of the measure representation of the  $D_{st}$  time series was provided in Wanliss *et al.* (2005). A prediction method was detailed in Anh *et al.* (2005) together with some numerical results evaluating its performance. A two-dimensional chaos game representation of the  $D_{st}$  index and prediction of geomagnetic storm events was proposed in Yu *et al.* (2007). The spatiotemporal scaling properties of the ground geomagnetic field variations from individual magnetometer stations were studied in Pulkkinen *et al.* (2005) and Cersosimo and

Wanliss (2007). Anh *et al.* (2007) used multifractal detrended fluctuation analysis (MF-DFA) to analyze ground magnetic fluctuations for the year 2000 Anno Domini. Yu *et al.* (2009) found the storm-flare class dependence through the measure representation (Yu *et al.* 2001a) and multifractal analysis.

In this paper, we will consider both high-latitude and low-latitude ground magnetometer measurements. We will use the data at 22 stations of the INTERMAGNET to investigate the scaling behaviour of both high and low latitudes.

The Earth's magnetic fluctuations are measured almost continuously by arrays of magnetometers located around the world. The INTERMAGNET program has established a global network of cooperating digital magnetic observatories that currently comprises over 108 observatories. Typical measured parameters include the north ( $B_x$ ) and east ( $B_y$ ) components of the horizontal intensity, and the vertical intensity ( $B_z$ ), or some combination of these. By constantly measuring the magnetic field through programs such as INTERMAGNET, we can observe how the field is changing over a period of years and use it to derive a mathematical representation of the Earth's magnetic field and how it is changing. It is noted that the  $D_{st}$  is calculated as an hourly average of the horizontal component  $B_x$  of the magnetic field at four observatories, namely, Hermanus ( $33.3^\circ$  south,  $80.3^\circ$  in magnetic dipole latitude and longitude), Kakioka ( $26.0^\circ$  north,  $206.0^\circ$ ), Honolulu ( $21.0^\circ$  north,  $266.4^\circ$ ), and San Juan ( $29.9^\circ$  north,  $3.2^\circ$ ). These four observatories were chosen because they are close to the magnetic equator and thus are not strongly influenced by auroral current systems. In this paper, we use the horizontal component  $B_x$  at 22 stations of INTERMAGNET covering 6 distinct regions, namely Southwest North America, Northeast North America, Central Europe, Northern Europe, Australasia and Asia. The stations and their geomagnetic latitudes are given in Table 2.

The time series of  $B_x$  at each station is modeled as the solution of a fractional stochastic differential equation (SDE) of the form (1) defined in the next section. A similar SDE was considered in Anh *et al.* (2008) to model the AE. A method to estimate the parameters of the model based on observed data was also given there. In this paper, we will pay particular attention to the degree of fractional differentiation  $\nu$  and the  $\alpha$ -stability index of the noise process  $L(t)$  driving Eq. (1). These two parameters, which express the scaling behaviour of the magnetic field at different locations, will be employed to cluster the stations. It will be seen that the  $B_x$  component possesses local trends, which must be removed before clustering can be performed. This trend removal will be carried out via an empirical mode decomposition. The parameter  $\nu$  is estimated by a detrended fluctuation analysis, while the parameter  $\alpha$  is obtained via Monte Carlo simulation of Eq. (1).

The next section details a description of Eq. (1) and the needed techniques of detrended fluctuation analysis and empirical mode decomposition. An estimation of Eq. (1) is then performed for each station. The numerical results are reported in Tables 1 and 2 in Section 3 for the cases of trend intact and trend removed respectively. It will be seen that the results for the case of trend removed are more consistent, hence will be used for station clustering. Consistency of the results is partially due to a good simulation of the observed  $B_x$  time series from the fractional SDEs. Hence a by-product of the approach of this paper is an efficient method and algorithm to simulate magnetometer time series via empirical mode decomposition and fractional SDE. A discussion of

the results and some conclusions will be given in Section 4.

## 2 Methods

### 2.1 $\alpha$ -stable distribution

The Lévy  $\alpha$ -stable distribution is defined by the Fourier transform of its characteristic function (Nolan 2009)

$$f(x; \alpha, \beta, \gamma, \delta) = \int_{-\infty}^{\infty} \varphi(t) e^{-itx} dt,$$

where  $\varphi(t)$  is given by

$$\varphi(t) = \exp\{i\delta t - \gamma|t|^\alpha[1 + i\beta \operatorname{sign}(t)w(t, \alpha)]\},$$

and

$$w(t, \alpha) = \begin{cases} \tan \frac{\alpha\pi}{2}, & \text{if } \alpha \neq 1, \\ \frac{2}{\pi} \log |t|, & \text{if } \alpha = 1, \end{cases}$$

$$\operatorname{sign}(t) = \begin{cases} 1, & \text{if } t > 0, \\ 0, & \text{if } t = 0, \\ -1, & \text{if } t < 0. \end{cases}$$

Here,  $\gamma$  is the scale parameter,  $\alpha$  the stability exponent,  $\delta$  the shift parameter and  $\beta$  the skewness parameter. The exponent  $\alpha$  controls the kurtosis and lies in the range  $(0, 2]$ . The value  $\alpha = 2$  corresponds to a Gaussian distribution (for any  $\beta$ ), while  $\alpha = 1$ ,  $\beta = 0$  corresponds to a Cauchy distribution. The skewness parameter  $\beta$  lies in the range  $[-1, 1]$ , and when it is zero, the distribution is symmetric and is referred to as a Lévy symmetric  $\alpha$ -stable distribution. The scale parameter  $\gamma$  must be larger than 0, and is equal to  $\frac{1}{2}$  of the variance in the Gaussian case ( $\alpha = 2$ ). The shift  $\delta$  is a location parameter; it is the mean when  $1 < \alpha \leq 2$  and the median when  $0 < \alpha < 1$  (Nikias and Shao 1995).

An empirical probability density function (PDF) can be computed from an observed time series. Then maximum likelihood can be used to estimate the parameters  $\alpha$ ,  $\beta$ ,  $\gamma$  and  $\delta$  in the  $\alpha$ -stable distribution and fit the empirical PDF of the time series.

### 2.2 Fractional stochastic differential equations driven by Lévy noise

Anh *et al.* (2008) provided a description of the non-Gaussianity and possible long-range dependence of the auroral electrojet (AE) index in the form of a fractional stochastic differential equation

$$\frac{dX}{dt} + \kappa \mathcal{D}^\nu X(t) = \eta \frac{dL}{dt}, \quad \nu \geq 0, \quad (1)$$

where the fractional derivative  $\mathcal{D}^\nu$  is defined by (Podlubny 1999, Eq. (2.138))

$$\mathcal{D}^\nu \xi(t) = \frac{1}{\Gamma(n - \nu)} \int_0^t (t - \tau)^{n - \nu - 1} \frac{d^n \xi(\tau)}{d\tau^n} d\tau, \quad (2)$$

$\nu \in [n-1, n)$ ,  $n = 1, 2, \dots$ ,  $\Gamma$  is the gamma function,  $\frac{dL}{dt}$  is Lévy noise defined in the distribution sense (see Mueller 1998, for example), and  $\kappa, \eta$  are constants. Specifically for ground magnetometer data, the Lévy noise of Eq. (1) is assumed to have an  $\alpha$ -stable distribution. Note that, for  $\nu = 0$  and  $\frac{dL}{dt} = \frac{dW}{dt}$ , Eq. (1) is the classical Langevin equation. If the value of  $\nu$  is equal to  $\frac{1}{2}$ , the equation for the time series then takes the form

$$\frac{dX}{dt} + \kappa \mathcal{D}^{\frac{1}{2}} X(t) = \eta \frac{dL}{dt}, \quad (3)$$

which is the Stokes-Boussinesq-Basset equation in hydrodynamics (driven by Gaussian noise).

We use a Lévy noise to drive Eq. (1). The  $\alpha$ -stable form of this Lévy process is suggested by the empirical probability density of the observed time series. The Green function solution of the fractional SDE (1) is obtained as

$$X(t) = \int_0^t G(t-s) dL(s), \quad (4)$$

where the Green function is given by

$$G(t) = E_{1-\nu, 1}(-\kappa t^{1-\nu}) \mathbf{1}_{(0, \infty)}(t), \quad 0 < \nu < 1,$$

with  $\mathbf{1}_{(0, \infty)}(t)$  being the indicator function, which is equal to 1 when  $t \in (0, \infty)$ , and is equal to 0 otherwise;  $E_{\nu, \rho}(x)$  being the two-parameter Mittag-Leffler function, which can be defined by the series expansion

$$E_{\nu, \rho}(x) = \sum_{k=0}^{\infty} \frac{z^k}{\Gamma(\nu k + \rho)}, \quad \nu > 0, \quad \rho > 0, \quad z \in \mathbb{C}.$$

It was derived in Anh and McVinish (2003) that the Green function of the SDE (1) is in fact

$$G(t) = \frac{1}{\pi} \int_0^{\infty} \frac{\kappa \lambda^{\nu} \sin(\nu \pi)}{\lambda^2 + \kappa^2 \lambda^{2\nu} + 2\kappa \lambda^{1+\nu} \cos(\pi(1-\nu))} e^{-t\lambda} d\lambda. \quad (5)$$

Note that this Green function has the form

$$G(t) = \int_0^{\infty} e^{-\lambda t} \mu(d\lambda), \quad (6)$$

with a finite Borel measure  $\mu(d\lambda) = \frac{1}{\pi} \frac{\kappa \lambda^{\nu} \sin(\nu \pi)}{\lambda^2 + \kappa^2 \lambda^{2\nu} + 2\kappa \lambda^{1+\nu} \cos(\pi(1-\nu))}$ . Hence, by Bernstein's theorem (Feller 1971),  $G(t)$  is a completely monotone function. This representation leads to an efficient method to simulate the solution of (4) as follows.

In view of (4) and (6), the solution of (1) is then given by

$$X(t) = \int_0^t \int_0^{\infty} e^{-\lambda(t-s)} \mu(d\lambda) dL(s). \quad (7)$$

It should be noted that  $\int_0^t e^{-\lambda(t-s)} dL(s)$  is the solution of the Ornstein-Uhlenbeck-type equation

$$dY(\lambda, t) = -\lambda Y(\lambda, t) dt + dL(t), \quad Y(\lambda, 0) = 0. \quad (8)$$

The following approximation scheme is given in Anh and McVinish (2003). Define a compact set  $K \subset [0, \infty)$  by  $K = [r^{-m}, r^n]$  with  $m, n$  being positive integers and  $r > 1$ . Denote the geometric

partition of  $K$  by  $\pi = \{A_i\}$  with  $A_i = [r^i, r^{i+1})$ ,  $i = -m, \dots, n-1$ . Consider the following approximation of  $X(t)$ :

$$X_\pi(t) = \sum_{\pi} \mu \{ [r^i, r^{i+1}) \} Y(r^i, t), \quad (9)$$

where  $Y(r^i, t)$  is the solution to the Ornstein-Uhlenbeck-type equation (8). Finally, the Ornstein-Uhlenbeck-type process is approximated by

$$Y_\Delta(t) = L(t), \quad (10)$$

for  $0 < t \leq \Delta$  and

$$Y_\Delta(t) = e^{-\lambda(t-(n-1)\Delta)} Y_\Delta((n-1)\Delta) + L(t) - L((n-1)\Delta), \quad (11)$$

for  $(n-1)\Delta < t \leq n\Delta$ . The approximation (9) of  $X(t)$  is then

$$X_{\pi,\Delta}(t) = \sum_{\pi} \mu \{ [r^i, r^{i+1}) \} Y_\Delta(r^i, t). \quad (12)$$

Suppose that  $K_N$  is a sequence of compact sets growing to  $(0, \infty)$ ,  $r_N \rightarrow 1$  and  $\Delta_N \rightarrow 0$  as  $N \rightarrow \infty$ . Then,

$$\sup_{t \leq T} |X(t) - X_{\pi,\Delta}(t)| \rightarrow 0$$

in mean square. The above approximation algorithm and convergence analysis were established in Anh and McVinish (2003). The algorithm plays an essential role in the estimation of the parameters of the SDE described below.

A way to simulate random variables from the  $\alpha$ -stable distribution is as follows (see Chambers *et al.* 1976):

(a) Generate  $V$  from a uniform distribution on  $[-\pi/2, \pi/2]$  and  $W$  from an exponential distribution with mean 1.

(b) For  $\alpha \neq 1$ , compute

$$X = S_{\alpha,\beta} \frac{\sin[\alpha(V + B_{\alpha,\beta})]}{[\cos(V)]^{1/\alpha}} \left[ \frac{\cos[V - \alpha(V + B_{\alpha,\beta})]}{W} \right]^{(1/\alpha-1)},$$

where

$$B_{\alpha,\beta} = \frac{\arctan(\beta \tan \frac{\pi\alpha}{2})}{\alpha},$$

$$S_{\alpha,\beta} = \left[ 1 + \beta^2 \tan^2 \left( \frac{\pi\alpha}{2} \right) \right]^{1/(2\alpha)};$$

for  $\alpha = 1$ , compute

$$X = \frac{2}{\pi} \left[ \left( \frac{\pi}{2} + \beta V \right) \tan V - \beta \ln \left( \frac{\pi W \cos V}{\pi + 2\beta V} \right) \right].$$

Then the stable variable  $Y$  can be computed as

$$Y = \begin{cases} \gamma X + \delta, & \text{if } \alpha \neq 1, \\ \gamma X + \frac{2}{\pi} \beta \gamma \ln \gamma + \delta, & \text{if } \alpha = 1. \end{cases}$$

Sample paths of the corresponding Lévy motion can then be generated as

$$L(nh) = \sum_{i=1}^n h^{1/\alpha} Y_i, \quad (13)$$

where the  $Y_i$  have an  $\alpha$ -stable distribution. This algorithm is needed in the simulation of paths of Eq. (1).

### 2.3 Detrended fluctuation analysis (DFA)

In order to estimate the order of fractional derivative, we performed a detrended fluctuation analysis (DFA) (Peng *et al.* 1994, Yu *et al.* 2001b, 2006, 2009) of the time series. The DFA is the special case when  $q = 2$  of the multifractal detrended fluctuation analysis (MF-DFA) detailed by Kantelhardt *et al.* (2002). We adopt the algorithm in Kantelhardt *et al.* (2002) and Movahed *et al.* (2006) to estimate the exponent of DFA in this paper. The procedure consists of five steps. Let  $\{X_k\}_{k=1}^N$  be a time series of length  $N$ .

*Step 1.* The time series is integrated as  $Y(i) = \sum_{k=1}^i [X_k - X_{ave}]$ ,  $i = 1, 2, \dots, N$ , where  $X_{ave}$  is the sample mean over the whole time period.

*Step 2.* The integrated time series is divided into  $N_s = [N/s]$  non-overlapping segments of equal length  $s$ . Here,  $[N/s]$  is the integer part of  $N/s$ . Since the length  $N$  of the series is often not a multiple of timescale  $s$ , a short part of length  $l_e = N - N_s s$  at the end of  $Y(i)$  may remain. In order not to disregard this part, the same procedure is repeated starting from the opposite end. Thereby,  $2N_s$  segments are obtained altogether.

*Step 3.* Calculate the local trend for each of the  $2N_s$  segments by a least squares fit of the series, then determine the variance

$$F^2(s, \nu) = \frac{1}{s} \sum_{i=1}^s \{Y[(\nu - 1)s + i] - y_\nu(i)\}^2, \quad (14)$$

for each segment  $\nu = 1, 2, \dots, N_s$ , and

$$F^2(s, \nu) = \frac{1}{s} \sum_{i=1}^s \{Y[(\nu - N_s - 1)s + i + l_e] - y_\nu(i)\}^2, \quad (15)$$

for each segment  $\nu = N_s + 1, N_s + 2, \dots, 2N_s$ . Here  $l_e = N - N_s s$ , and  $y_\nu(i)$  is the fitting linear polynomial in the  $\nu$ th segment.

*Step 4.* Average over all segments to get the second-order fluctuation function

$$F(s) = \left\{ \frac{1}{2N_s} \sum_{\nu=1}^{2N_s} [F^2(s, \nu)] \right\}^{1/2}. \quad (16)$$

By construction,  $F(s)$  is only defined for  $s \geq 3$ .

*Step 5.* Determine the scaling behavior of the fluctuation function by analyzing log-log plots of  $F(s)$  versus  $s$ , i.e., the power law

$$F(s) \propto s^h, \quad (17)$$

in some range of time scale  $s$ .

For model (1), Anh *et al.* (2008) suggested a method to estimate the fractional order  $\nu$  based on an estimation of the scaling exponent  $h$ , namely, via the relationship  $\nu = h - \frac{1}{2}$ .

## 2.4 Algorithm for simulation of fractional SDE

First, the empirical PDF of the given time series is computed. We denote this empirical PDF as  $f_0(x)$ . The parameters  $\alpha$ ,  $\beta$ ,  $\gamma$  and  $\delta$  of the  $\alpha$ -stable distribution are then estimated via maximum likelihood. Then we use the DFA to estimate the parameter  $h$  and get an estimate for the parameter  $\nu$  via the relationship  $\nu = h - 1/2$ . We fix these estimated values for  $\alpha$ ,  $\beta$ ,  $\gamma$ ,  $\delta$  and  $\nu$  in the SDE (1). Setting initial values for  $\kappa$  and  $\eta$ , we then generate a sample path of the process  $X(t)$  defined by (7) via the approximation algorithm described by (9) - (12). Another empirical PDF based on this path of  $X(t)$  is then computed.

The procedure is continued for different sets of values of the parameters  $(\kappa, \eta)$ , and we denote the resulting empirical PDF as  $\hat{f}(x)$ . The estimates of the parameters of Eq. (1) are those corresponding to

$$\min_{\kappa, \eta} \sum_{i=1}^N \left( f_0(x_i) - \hat{f}(x_i) \right)^2, \quad (18)$$

where  $N$  is the number of points on the pdf curve we selected. In this paper, we set  $N = 130$ .

We solve problem (18) by using the function *fminsearch* in MATLAB version 7.1. This algorithm finds the minimum of a scalar function of several variables based on the Nelder-Mead simplex search method (Lagarias *et al.* 1998). It should be noted that the PDF  $\hat{f}(x)$  may have to be computed for a large number of times, once for each new set of parameters, before the minimum is reached.

A solution path of Eq. (1) based on these estimates is generated. To compare the patterns of the original and simulated series, we replaced values higher than the maximum value or less than the minimum value of the original time series by a uniformly random number between the minimum value and the maximum value.

## 2.5 Empirical mode decomposition

Lin *et al.* (2009) described the traditional empirical mode decomposition (EMD) and presented a new approach to EMD. We outline some content of Lin *et al.* (2009) here. The traditional EMD for data, which is a highly adaptive scheme serving as a complement to Fourier and wavelet transforms, was originally proposed by Huang *et al.* (1998). In EMD a complicated data set is decomposed into a finite, often small, number of components called *intrinsic mode functions* (IMF), which seem to admit well behaved Hilbert transforms. EMD has been used successfully in many applications in analyzing a diverse range of data sets in biological and medical sciences, geology, astronomy, engineering, etc. (e.g., Janosi and Muller 2005; Shi *et al.* 2008).

The original EMD is obtained through a shifting algorithm: Let  $\{t_j\}$  be the local maxima of a signal  $X(t)$ . The cubic spline  $E_U(t)$  connecting the points  $\{(t_j, X(t_j))\}$  is referred to as the *upper envelope* of  $X$ . The *lower envelope*  $E_L(t)$  is similarly obtained from the local minima  $\{s_j\}$  of  $X(t)$ . Then we define the operator  $\mathcal{S}$  by

$$\mathcal{S}(X) = X - \frac{1}{2}(E_U + E_L).$$

In the so-called *sifting algorithm*, the first IMF in the EMD is given by

$$I_1 = \lim_{n \rightarrow \infty} \mathcal{S}^n(X).$$

Subsequent IMFs in the EMD are obtained recursively via

$$I_k = \lim_{n \rightarrow \infty} \mathcal{S}^n(X - I_1 - \dots - I_{k-1}).$$

The process stops when  $Y = X - I_1 - I_2 - \dots - I_m$  has at most one local maximum or local minimum. This function  $Y(t)$  denotes the local trend in  $X(t)$ .

Lin *et al.* (2009) proposed a new algorithm called *iterative filtering* for EMD. Instead of using the envelopes generated by spline. In this new algorithm a low-pass filter is used to generate a moving average to replace the mean of the envelopes. The essence of the sifting algorithm remains. Let  $\mathcal{L}$  be an operator that is a low-pass filter, for which  $\mathcal{L}(X)(t)$  represent the moving average of  $X$ . We now define

$$\mathcal{T}(X) = X - \mathcal{L}(X).$$

In this approach, the low-pass filter  $\mathcal{L}$  is dependent on the data  $X$ . For a given  $X(t)$  we choose a low-pass filter  $\mathcal{L}_1$  accordingly and set  $\mathcal{T}_1 = I - \mathcal{L}_1$ , where  $I$  is the identity operator. The first IMF in the new EMD is given by  $\lim_{n \rightarrow \infty} \mathcal{T}_1^n(X)$ , and subsequently the  $k$ -th IMF  $I_k$  is obtained first by selecting a low-pass filter  $\mathcal{L}_k$  according to the data  $X - I_1 - \dots - I_{k-1}$  and iterations  $I_k = \lim_{n \rightarrow \infty} \mathcal{T}_k^n(X - I_1 - \dots - I_{k-1})$ , where  $\mathcal{T}_k = I - \mathcal{L}_k$ . Again the process stops when  $Y = X - I_1 - \dots - I_m$  has at most one local maximum or local minimum. Lin *et al.* (2009) suggested to use the filter  $Y = \mathcal{L}(X)$  having the form  $Y(n) = \sum_{j=-m}^m a_j X(n+j)$  and proved the convergence of the sifting algorithm for a class of filters. We choose the filter given by  $a_j = \frac{m-|j|+1}{m+1}$ ,  $j = -m, \dots, m$  for this study, which is simple but works well and is shown to converge.

**Hilbert transform:** having obtained the IMFs (denoted as  $I_k$ ), one will have no difficulty in applying the Hilbert transform to each IMF component,

$$\mathcal{H}(I_k(t)) = \frac{1}{\pi} PV \int_{-\infty}^{\infty} \frac{I_k(t)}{t - \tau} d\tau,$$

in which the PV indicates the principle value of the singular integral. Then the instantaneous amplitude is defined as (Shi *et al.* 2008)

$$r_k(t) = \sqrt{I_k^2(t) + \mathcal{H}^2(I_k(t))}.$$

Shi *et al.* (2008) considered IMF2, IMF3, IMF4 and defined the energy value as  $e_k = \sum_t r_k(t)$ ,  $k = 2, 3, 4$ , and then used the energy ratio  $g_k = \frac{e_k}{e_2 + e_3 + e_4}$ ,  $k = 2, 3, 4$  to predict protein subcellular location.

### 3 Data analysis and discussion

We use the above methods to model the hourly averaged magnetic field time series  $B_x$  from 22 INTERMAGNET stations. We collect the stations into 6 groups for the year 2000 A.D.: Southwest North America (NA1), Northeast North America (NA2), Central Europe (CEUR), Northern Europe (NEUR), Australasia (AUS) and Asia (ASIA). The stations in each group are listed in Table 1. Figure 1 shows the time series from the BOU station in NA1 as an example to illustrate the typical anomalous nature of this kind of data. This  $B_x$  time series clearly displays non-Gaussianity at large

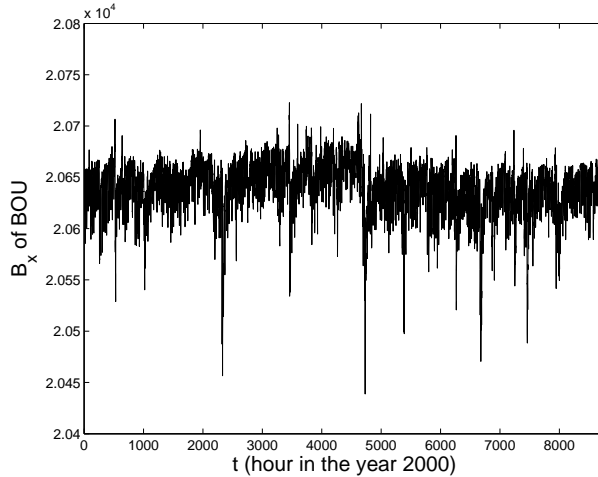


Figure 1: The hourly magnetic field  $B_x$  component for the year 2000 at station BOU.

scales and Brownian motion-type behavior at small scales. This indicates the existence of different scalings in the process.

The empirical density of this time series, as shown in Figure 2, is consistent with a skewed  $\alpha$ -stable distribution. Hence we used maximum likelihood (implemented by the program STABLE downloaded from J. P. Nolan's website: <http://www.academic2.american.edu/jpnolan>) to estimate the parameters  $\alpha$ ,  $\beta$ ,  $\gamma$  and  $\delta$  in the  $\alpha$ -stable distribution and generate the corresponding PDF to fit the empirical density of the observed time series. We found that the  $\alpha$ -stable distribution provides a reasonably good fit to the probability density of  $B_x$  data (see Figure 2). The estimated values of  $\alpha$ ,  $\beta$ ,  $\gamma$  and  $\delta$  for  $B_x$  of these stations are given in Table 1.

Then we performed a detrended fluctuation analysis on the  $B_x$  data. For the given time series, we found good linear relationships of  $\log_{10} F(s)$  versus  $\log_{10} s$  in the time scale range of  $5 \leq s \leq 25$  hours (almost a day). The estimated values of the exponent  $h$  for  $B_x$  are given in Table 1. For example, the DFA slope estimation for the  $B_x$  at the BOU station is given in Figure 3. The  $h$  values of the  $B_x$  time series, which vary in the range  $1.0 < h < 1.5$ , indicate that the observed  $B_x$  time series are non-stationary and anti-persistent.

Then we tried to simulate paths of  $B_x$  using the fractional SDE (1) directly, but found that all the resulting simulations are not adequate; in particular, they were not able to trace the local trends, which are pronounced in the magnetic field data. So we used the traditional EMD (Huang *et al.* 1998) and the new EMD developed by Lin *et al.* (2009) to fit these local trends. We found that both EMDs can fit the trends well, but the new EMD works slightly better. Hence we just showed the results using the new EMD in the following. We used the new EMD to get the IMFs as in Figure 4, which show that the randomness becomes less from IMF1 to IMF4, and IMF4 is relatively smooth. Hence we define the local trend of the magnetic field data as  $Y = X - (IMF1 + IMF2 + IMF3 + IMF4)$ . We then removed the local trend from the raw data by  $X - Y$  to get the detrended data  $(IMF1 + IMF2 + IMF3 + IMF4)$ , which appear to be stationary. For example, we fit the local trend of  $B_x$  data at the BOU station in the upper panel of Figure 5 and get the detrended data in the lower panel of Figure 5.

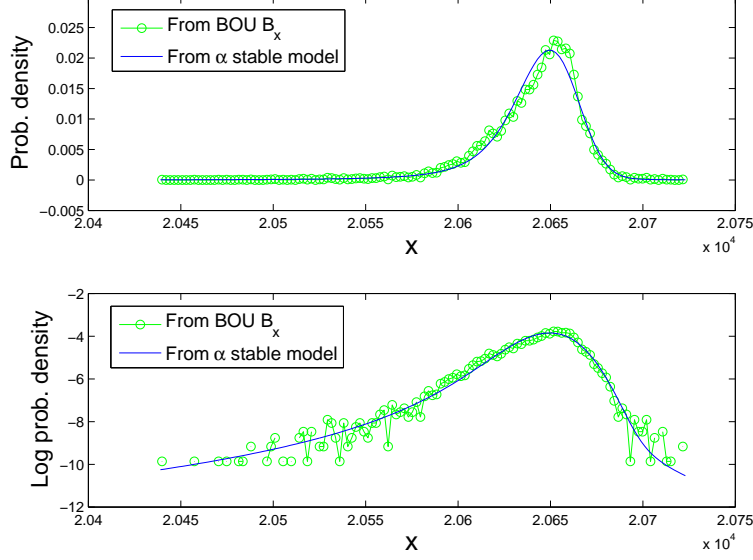


Figure 2:  $\alpha$ -stable distribution fit for the probability density of hourly magnetic field component  $B_x$  at station BOU

Table 1: The estimated values of  $\alpha$ ,  $\beta$ ,  $\gamma$  and  $\delta$  when we use the  $\alpha$ -stable distribution to fit the probability density, and the power law exponent  $h$  in DFA of the  $B_x$  data at the selected stations.

Group	Station	$\min(B_x)$	$\max(B_x)$	$\alpha$	$\beta$	$\gamma$	$\delta$	$h$
NA1	BOU	20439	20723	1.5879	-0.8989	13.1886	20648.1	$1.1959 \pm 0.0334$
	FRN	22767	23174	1.6511	-0.9008	13.6125	23090.4	$1.2217 \pm 0.0265$
	DLR	24996	25366	1.7012	-0.9900	15.8343	25288.5	$1.2481 \pm 0.0294$
	TUC	24213	24596	1.7114	-0.9900	15.5121	24515.8	$1.2492 \pm 0.0239$
NA2	FCC	7388.4	9283.7	1.2705	-0.3183	37.4423	8440.47	$1.2188 \pm 0.0227$
	PBQ	10022	12144	1.2703	-0.3248	31.9522	11031.1	$1.2249 \pm 0.0218$
	OTT	16422	17823	1.6929	-0.8602	18.0112	16967.4	$1.1738 \pm 0.0723$
	STJ	17540	18266	1.6525	-0.9253	18.3224	17914.7	$1.2192 \pm 0.0532$
CEUR	BDV	20052	20399	1.5927	-0.8663	11.4755	20296.9	$1.3191 \pm 0.0300$
	NCK	20814	21127	1.6256	-0.8641	10.9772	21040.3	$1.3010 \pm 0.0291$
	FUR	20608	20939	1.5815	-0.8700	11.2065	20842.9	$1.3148 \pm 0.0275$
	NGK	18455	18930	1.6334	-0.8597	12.1750	18780.0	$1.2998 \pm 0.0362$
NEUR	ABK	10189	12258	0.9401	-0.1305	19.9918	11455.2	$1.2200 \pm 0.0292$
	NUR	14041	15352	1.5973	-0.3771	13.1472	14897.1	$1.2058 \pm 0.0672$
	LOV	14531	15664	1.6463	-0.4805	12.8191	15297.0	$1.2167 \pm 0.0664$
	SOD	10129	12277	0.9829	-0.1366	17.0264	11477.4	$1.2122 \pm 0.0319$
AUS	ASP	29665	30014	1.6334	-0.8627	13.6621	29940.2	$1.3426 \pm 0.0171$
	CTA	31239	31617	1.6017	-0.8537	13.6192	31529.0	$1.3500 \pm 0.0233$
	KDU	35056	35470	1.7123	-0.3080	16.8851	35357.8	$1.4698 \pm 0.0468$
ASIA	BMT	28170	28528	1.6517	-0.9435	14.2766	28457.1	$1.2653 \pm 0.0330$
	KAK	29520	29867	1.6464	-0.8909	13.9227	29785.2	$1.3146 \pm 0.0273$
	MMB	25584	25952	1.6389	-0.9450	14.1416	25877.4	$1.2761 \pm 0.0367$

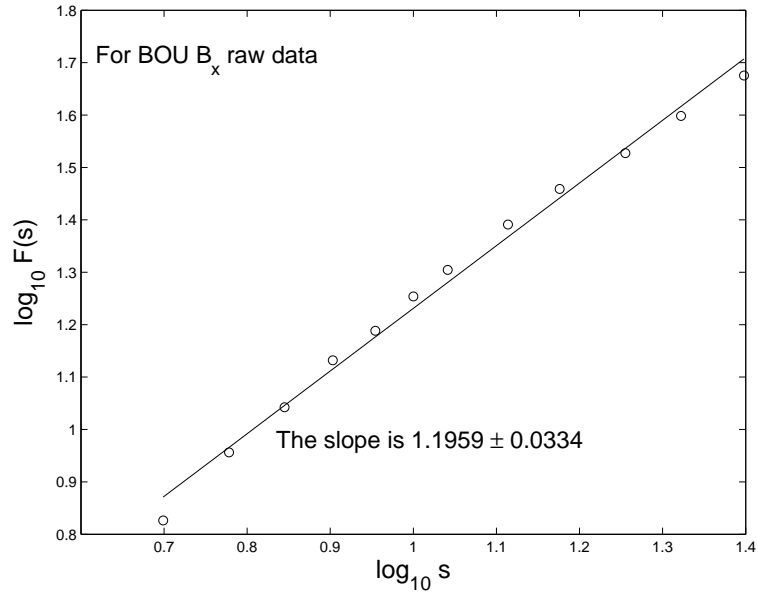


Figure 3: The DFA slope estimation for the  $B_x$  data of BOU station.

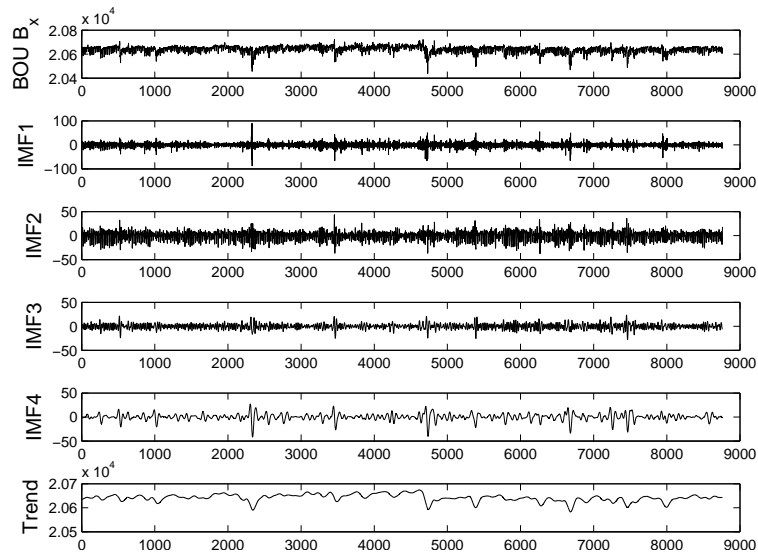


Figure 4: The EMD results of the  $B_x$  data of BOU station.

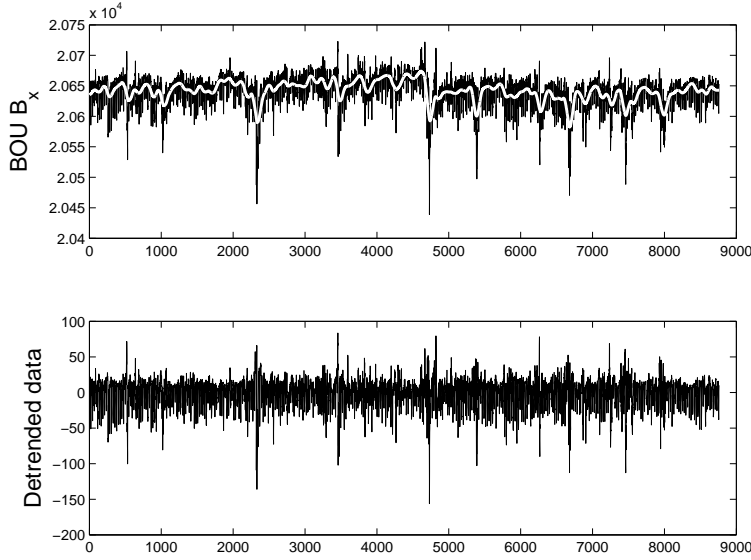


Figure 5: The local trend (white curve) of  $B_x$  data in BOU station ( upper panel) and the detrended data (lower panel).

We now use the fractional SDE (1) to simulate the detrended data ( $IMF1 + IMF2 + IMF3 + IMF4$ ). We found that the fractional SDE simulates very well all detrended  $B_x$  time series. The next step is to fit the empirical density of the detrended data using an  $\alpha$ -stable distribution. Then we used the slope of DFA in the time scale range  $11 \leq s \leq 47$ , which gives good linear relationships, to infer the exponent  $h$  and get an estimate of the parameter  $\nu$  via the relationship  $\nu = h - 1/2$ . We then fixed the estimated values of the parameters  $\alpha, \beta, \gamma, \delta$  and  $\nu$  in the SDE (1) and used the simulation algorithm in Section 2.4 to estimate the coefficients  $\kappa$  and  $\eta$  via (18). The estimated values of all the parameters  $\alpha, \beta, \gamma$  and  $\delta, \nu, \kappa$  and  $\eta$  for the detrended  $B_x$  at the selected stations are listed in Table 2.

From these estimates of all the parameters, we simulated sample paths of detrended data, denoted as  $\hat{X}_{detrend}$ . A simulation of each time series  $B_x$  is then obtained as the sum of such a simulated path  $\hat{X}_{detrend}$  and the fitted trend  $Y$ . As an example, we show the simulation of the  $B_x$  time series at the BOU station in the left column of Figure 6 and the corresponding empirical density of the detrended data in its right column. It is seen that the empirical density generated from the fractional SDE follows the tails of the detrended  $B_x$  series, while the positive tail generated from the theoretical  $\alpha$ -stable density is thinner but longer than that of the empirical density. More examples of the simulation of  $B_x$  time series are given in Figure 7.

The simulated paths trace very well those of the observed time series. In conjunction with excellent fitting of the empirical densities of the time series, the results indicate that the fractional SDE (1) in combination with empirical mode decomposition provides a good method to model the components of the magnetic field. In fact, we tried the method on the  $B_y$  and  $B_z$  components and the simulations are equally excellent for all 22 stations.

For the purpose of clustering of the magnetic field, the two most significant parameters are the stability exponent  $\alpha$  and the degree of differentiation  $\nu$  (or  $h$  as reported). As was proved in

Table 2: The estimated values of  $\alpha$ ,  $\beta$ ,  $\gamma$  and  $\delta$  when we use the  $\alpha$ -stable distribution to fit the probability density, and the power law exponent  $h$  in DFA, estimated  $\kappa$  and  $\eta$  of the detrended  $B_x$  data at the selected stations. We set 1.5 and 2.5 as the initial value of  $\kappa$  and  $\eta$  respectively for all stations except FCC (1.5,1.0), ABK (1.5,1.0) and SOD (2.0,1.0).

Group	Station	Geomagnetic latitude ( $^\circ$ )	$\alpha$	$\beta$	$\gamma$	$\delta$	$h$	$\kappa$	$\eta$
NA1	BOU	40.14	1.5237	-0.8341	9.98987	5.10507	$0.8884 \pm 0.0321$	1.7100	2.2923
	FRN	37.09	1.6169	-0.6796	9.75016	3.42546	$0.9423 \pm 0.0217$	1.4137	2.6347
	DLR	29.49	1.5925	-0.4920	9.30300	2.84548	$1.0046 \pm 0.0159$	0.7182	3.8897
	TUC	32.17	1.6118	-0.4884	9.31218	2.59578	$0.9905 \pm 0.0158$	1.5345	2.5371
NA2	FCC	58.76	1.2604	-0.1740	35.7932	11.1448	$0.7891 \pm 0.0516$	1.3490	1.1252
	PBQ	55.28	1.1022	-0.0650	25.2671	7.05106	$0.8242 \pm 0.0579$	1.3962	1.0606
	OTT	45.40	1.3143	-0.7016	10.5020	6.61395	$0.7508 \pm 0.0325$	1.4977	1.0506
	STJ	47.60	1.3946	-0.7397	9.76454	6.00033	$0.7595 \pm 0.0354$	1.4586	1.0410
CEUR	BDV	49.08	1.5513	-0.5706	8.53128	3.08720	$0.9432 \pm 0.0340$	1.2553	2.9598
	NCK	47.63	1.5359	-0.5312	7.58381	2.74455	$0.9617 \pm 0.0313$	1.4121	2.6619
	FUR	48.16	1.5457	-0.5333	8.24641	2.90425	$0.9544 \pm 0.0330$	0.9244	2.9225
	NGK	52.07	1.5809	-0.6605	9.52715	3.45741	$0.8771 \pm 0.0376$	1.4525	2.5750
NEUR	ABK	68.36	1.0559	-0.0396	25.2279	6.86519	$0.7397 \pm 0.0496$	1.6266	0.9744
	NUR	60.51	1.3905	-0.3972	10.2271	3.66515	$0.7346 \pm 0.0385$	1.4555	1.0791
	LOV	59.90	1.4335	-0.4894	9.81644	3.82705	$0.7433 \pm 0.0387$	1.5036	1.0878
	SOD	67.37	1.0434	-0.0085	20.0871	5.14762	$0.7340 \pm 0.0471$	1.8166	1.1511
AUS	ASP	-23.76	1.6202	-0.2351	9.77916	1.85506	$1.1191 \pm 0.0238$	0.6305	4.4862
	CTA	-20.09	1.5271	-0.0957	9.43664	1.51390	$1.1411 \pm 0.0298$	1.5642	2.5204
	KDU	-12.69	1.5580	0.2269	12.9957	-0.77396	$1.0145 \pm 0.0397$	1.4929	2.3166
ASIA	BMT	40.34	1.5994	-0.5864	10.1863	3.48716	$0.9914 \pm 0.0249$	1.3488	2.7529
	KAK	36.23	1.6003	-0.3849	9.30575	2.41755	$1.0954 \pm 0.0273$	1.2019	2.7582
	MMB	43.91	1.5712	-0.6727	10.2512	4.06109	$0.9737 \pm 0.0382$	1.2852	2.7394

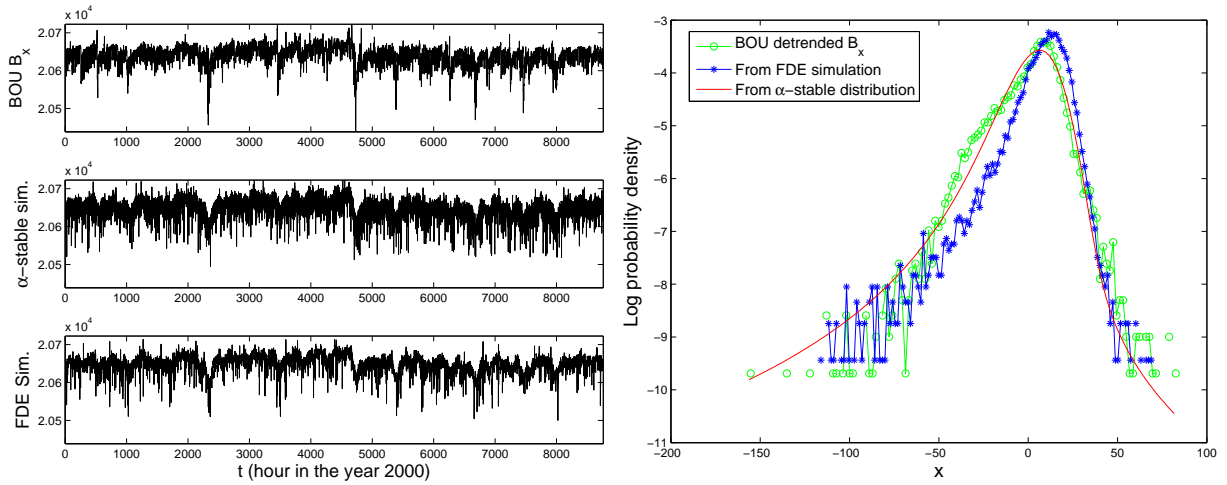


Figure 6: **(Left)**: The SDE simulation of the  $B_x$  data at BOU station. **(Right)**: the corresponding probability density of the detrended data.

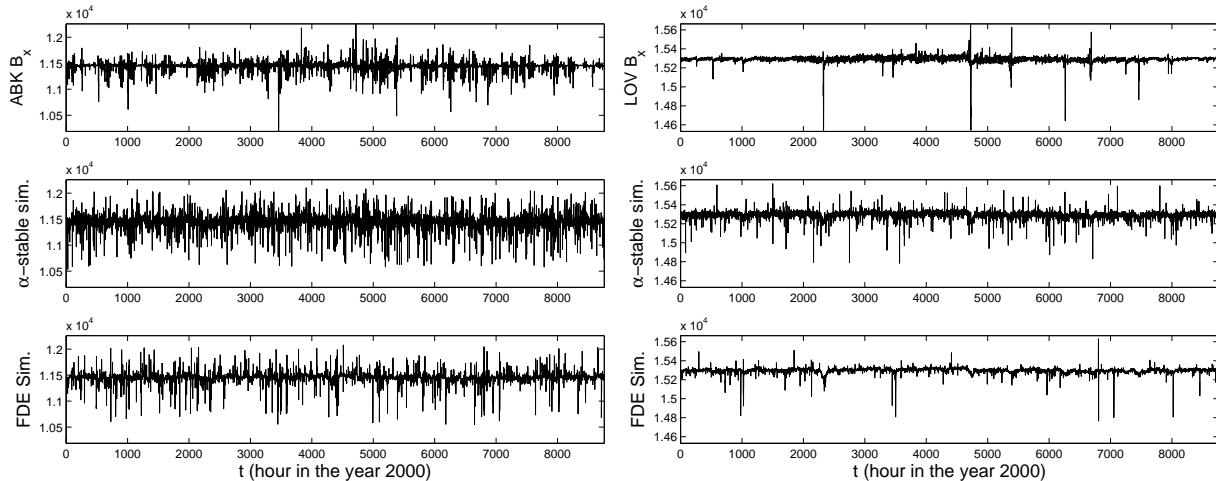


Figure 7: **(Left)**: The SDE simulation of the  $B_x$  data at ABK station. **(Right)**: The SDE simulation of the  $B_x$  data at ABK station.

Jaffard (1999), the paths of an  $\alpha$ -stable process is multifractal, while, the degree of differentiation  $\nu$  indicates the extent of self-similarity in the process.

Using the estimates of  $\alpha$  reported in Table 2, it is seen that the stations group into two distinct regions, one consisting of NA1, CEUR, AUS and ASIA corresponding to  $\alpha = 1.6$  approximately, and the other consisting of NA2 and NEUR corresponding to  $\alpha = 1.3$  approximately. It is noted that NEUR is composed of those stations above  $60^\circ N$  and NA2 is composed of those stations of Northeast America around  $60^\circ N$ . The values of  $h$  reported in Table 1 also confirm the clustering of these two regions corresponding to  $h = 1$  and  $h = 0.75$  approximately. We recall that  $\alpha$  signifies the degree of non-Gaussianity (away from Gaussianity, which corresponds to  $\alpha = 2$ ). The smaller value of  $\alpha = 1.3$  shows a higher degree of fluctuations in the magnetometer measurements at the stations of NA2 and NEUR. This is corroborated by a smaller  $h$  value, meaning a smaller extent of self-similarity/memory, for NA2 and NEUR.

Another outcome from the numerical results is that these estimates for  $\alpha$  and  $h$  remain approximately constant in these two regions, implying that their fluctuations be driven by two different sources.

## 4 Conclusions

The numerical results from detrended fluctuation analysis show that the magnetic field time series are non-stationary and anti-persistent, consistent with this type of geophysical data. The  $\alpha$ -stable density fits the empirical densities of magnetic field time series very well. The time series have pronounced local trends. Empirical mode decomposition is found to be a suitable technique to fit this type of local trends. These local trends must be removed before a fractional SDE can be developed. It is seen that the probability density generated from such a fractional SDE follows closely that of a detrended  $B_x$  series, while the tail of the theoretical  $\alpha$ -stable density is continuous and longer, hence generating a denser path of extreme values. It is also found that fractional SDEs

simulate very well detrended magnetic field time series.

The main finding of this paper is the presence of two distinct scaling regimes, one in the low latitudes near the equator similar to that of the  $D_{st}$ , and the other above latitude  $60^\circ N$  consistent with that of the AE. These scalings are characteristic of each region, which maps into the inner magnetosphere and the magnetospheric region related to the solar wind respectively. The scalings are fairly constant, confirming these two different sources in driving the fluctuations in the magnetic field.

The numerical results of the  $\alpha$ -stability index and the self-similarity index indicate that the intrinsic dynamics of the low-latitude magnetosphere is less complex than the high-latitude magnetosphere. This supports Wanliss and Reynolds (2003)'s suggestion that the result may help quantify the dynamics of the inner magnetosphere itself without the direct presence of the solar wind driver.

## Acknowledgements

This research was partially supported by the Australian Research Council grant DP0559807, the National Science Foundation grants ATM-0449403, DMS-0813750, the Chinese Program for New Century Excellent Talents in University grant NCET-08-06867 and the Fok Ying Tung Education Foundation grant 101004.

## References

- V.V. Anh and R. McVinish, Fractional differential equations driven by Lévy noise, *J. Applied Mathematics and Stochastic Analysis*, **16** (2003) 97-119.
- V.V. Anh, J.M. Yong and Z.G. Yu, Stochastic modeling of the auroral electrojet index, *J. Geophys. Res.*, **113** (2008) A10215, doi:10.1029/2007JA012851.
- V.V. Anh, Z.G. Yu and J.A. Wanliss, Analysis of global geomagnetic variability, *Nonlinear Processes in Geophysics*, **14** (2007) 701-708.
- V.V. Anh, Z.G. Yu, J.A. Wanliss and S.M. Watson, Prediction of magnetic storm events using the  $D_{st}$  index, *Nonlinear Processes in Geophysics*, **12** (2005) 799-806.
- L.F. Burlaga, Multifractal structure of the interplanetary magnetic field: Voyager 2 observations near 25 AU, 1987-1988, *Geophys. Res. Lett.*, **18**(1) (1991) 69-72.
- L.F. Burlaga, Lognormal and multifractal distributions of the heliospheric magnetic field, *J. Geophys. Res.*, **106** (2001) 15917-15927.
- L.F. Burlaga, C. Wang and N.F. Ness, A model and observations of the multifractal spectrum of the heliospheric magnetic field strength fluctuations near 40 AU, *Geophys. Res. Lett.*, **30** (2003) 1543, doi:10.1029/2003GL016903.
- D.O. Cersosimo, and J.A. Wanliss, Initial studies of high latitude magnetic field data during different magnetospheric conditions, *Earth Planets Space*, **59** (1) (2007) 39-43.
- J.M. Chambers, C.L. Mallows, and B.W. Stuck, A method for simulating stable random variables, *Journal of the American Statistical Association*, **71** (1976) 340-344.
- T.S. Chang, Self-organized criticality, multi-fractal spectra, sporadic localized reconnections and intermittent turbulence in the magnetotail, *Phys. Plasmas*, **6** (1999) 4137-4145.
- S.C. Chapman, N.W. Watkins, R.O. Dendy, P. Helander and G. Rowlands, A simple avalanche model as an analogue for magnetospheric activity, *Geophys. Res. Lett.*, **25** (1998) 2397-2400.

- G. Consolini, M.F. Marcucci and M. Candidi, Multifractal structure of auroral electrojet index data, *Phys. Rev. Lett.*, **76** (1996) 4082-4085.
- W. Feller, *An Introduction to Probability Theory and its Applications*, Wiley, 1971.
- M.P. Freeman and N.W. Watkins, The heavens in a pile of sand, *Science*, **298** (2002) 979-980.
- N. Huang, Z. Shen, S.R. Long, M.L. Wu, H.H. Shih, Q. Zheng, N.C. Yen, C.C. Tung and H.H. Liu, The empirical mode decomposition and Hilbert spectrum for nonlinear and nonstationary time series analysis. *Proc. Roy. Soc. London A*, **454** (1998) 903-995.
- S. Jaffard, The multifractal nature of Lévy processes, *Probability Theory and Related Fields*, **114** (1999) 207-227.
- I.M. Janosi and R. Muller, Empirical mode decomposition and correlation properties of long daily ozone records, *Phys. Rev. E*, **71** (2005) 056126 (p1-p5).
- K. Kabin and V.O. Papitashvili, Fractal properties of the IMF and the Earth's magnetotail field, *Earth Planets Space*, **50** (1998) 87-90.
- J.W. Kantelhardt, S.A. Zschiegner, E. Koscielny-Bunde, A. Bunde, S. Havlin and H.E. Stanley, Multifractal detrended fluctuation analysis of nonstationary time series, *Physica A*, **316** (2002) 87-114.
- A.J. Klimas, V. M. Uritsky, D. Vassiliadis and D. N. Baker, Reconnection and scale-free avalanching in a driven current-sheet model, *J. Geophys. Res.* **109** (2004) A02218.
- J.C. Lagarias, J.A. Reeds, M.H. Wright and P.E. Wright, Convergence properties of the Nelder-Mead simplex method in low dimensions, *SIAM Journal of Optimization*, **9** (1998) 112-147.
- L. Lin, Y. Wang and H. Zhou, Iterative filtering as an alternative for empirical mode decomposition, *Advances in Adaptive Data Analysis*, **1** No. 4 (2009), 543-560.
- A.T.Y. Lui, Multiscale phenomena in the near-Earth magnetosphere, *J. Atmos. Sol.-Terr. Phys.*, **64** (2002) 125-143.
- A.T.Y. Lui, S.C. Chapman, K. Liou, P.T. Newell, C.I. Meng, M. Brittnacher and G.K. Parks, Is the dynamic magnetosphere an avalanching system? *Geophys. Res. Lett.*, **27** (2000) 911-914.
- A.T.Y. Lui, W.W. Lai, K. Liou and C.I. Meng, A new technique for short-term forecast of auroral activity, *Geophys. Res. Lett.*, **30** (2003) 1258, doi:10.1029/2002GL016505.
- M.S. Movahed, G.R. Jafari, F. Ghasemi, S. Rahvar and M.R.R. Tabar, Multifractal detrended fluctuation analysis of sunspot time series, *J. Stat. Mech.: Theory exper.*, **2** (2006) P02003, doi:10.1088/1742-5468/2006/02/P02003.
- C. Mueller, The heat equation with Lévy noise, *Stoch. Proc. Appl.* **74** (1998) 67-82.
- C.L. Nikias and M. Shao, *Signal processing with alpha-stable distributions and applications*, John Wiley & Sons, INC, 1995.
- J. P. Nolan, *Stable Distributions - Models for Heavy Tailed Data*, Birkhäuser, Boston, 2009. In progress, Chapter 1 online at [academic2.american.edu/~jpnolan](http://academic2.american.edu/~jpnolan).
- C.-K. Peng, S. V. Buldyrev, S. Havlin, M. Simons, H. E. Stanley, and A. L. Goldberger, Mosaic organization of DNA nucleotides, *Phys. Rev. E*, **49** (1994) 1685-1689.
- I. Podlubny, *Fractional Differential Equations*, Academic Press, 1999.
- A. Pulkkinen, A. Klimas, D. Vassiliadis and V. Uritsky, Role of stochastic fluctuations in the magnetosphere-ionosphere system: A stochastic model for the AE index variations, *J. Geophys. Res.* **111** (2006) A10218.
- A. Pulkkinen, A. Klimas, D. Vassiliadis, V. Uritsky, and E. Tanskanen, Spatiotemporal scaling properties of the ground geomagnetic field variations, *J. Geophys. Res.*, **111** (2005) A03305, doi:10.1029/2005JA011294.
- F. Shi, Q.J. Chen and N.N. Li, Hilbert Huang transform for predicting proteins subcellular location. *J. Biomedical Science and Engineering*, **1** (2008) 59-63.
- V.M. Uritsky, A. J. Klimas, D. Vassiliadis, D. Chua, G. Parks, Scale-free statistics of spatiotemporal auroral emissions as depicted by POLAR UVI images: Dynamic magnetosphere is an avalanching system, *J. Geophys. Res.* **107** (2002) A12, 1426.
- V.M. Uritsky and M.I. Pudovkin, Low frequency  $1/f$ -like fluctuations of the AE index as a possible manifestation of self-organized criticality in the magnetosphere, *Annales Geophysicae*, **16** (1998) 1580-1588.
- J.A. Wanliss, Nonlinear variability of SYM-H over two solar cycles, *Earth Planets Space*, **56** (2004) e13-16.
- J.A. Wanliss, Fractal properties of SYM-H during quiet and active times, *J. Geophys. Res.*, **110** (2005) A03202, doi:10.1029/2004JA010544.

J.A. Wanliss, V.V. Anh, Z.G. Yu and S. Watson, Multifractal modelling of magnetic storms via symbolic dynamics analysis, *J. Geophys. Res.*, **110** (2005) A08214, doi:10.1029/2004JA010996.

J.A. Wanliss and P. Dobias, Space Storm as a Phase Transition, *J. Atmos. Sol. Terr. Phys.*, **69** (2007) 675-684, doi:10.1016/j.jastp.2007.01.001.

J.A. Wanliss and M.A. Reynolds, Measurement of the stochasticity of low-latitude geomagnetic temporal variations, *Annals Geophysicae*, **21** (2003) 2025-2030.

N.W. Watkins, D. Credgington, B. Hnat, S.C. Chapman, M. Freeman and J. Greenhough, Towards synthesis of solar wind and geomagnetic scaling exponents: a fractional Lévy motion model, *Space Science Reviews*, **121** (2005) 271-284.

Z. G. Yu, V. Anh and K.S. Lau, Measure representation and multifractal analysis of complete genome, *Phys. Rev. E*, **64** (2001a) 31903.

Z.G. Yu, V.V. Anh, K.S. Lau and L.Q. Zhou, Fractal and multifractal analysis of hydrophobic free energies and solvent accessibilities in proteins, *Phys. Rev. E*, **63** (2006) 031920.

Z.G. Yu, V. Anh and R. Eastes, Multifractal analysis of geomagnetic storm and solar flare indices and their class dependence, *J. Geophys. Res.* **114** (2009) A05214, doi: 10.1029/2008JA013854.

Z.G. Yu, V.Anh and B. Wang , Correlation property of length sequences based on global structure of complete genome, *Phys. Rev. E*, **63** (2001b) 011903.

Z.G. Yu, V.V. Anh, J.A. Wanliss, and S.M. Watson, Chaos game representation of the Dst index and prediction of geomagnetic storm events, *Chaos, Solitons and Fractals*, **31** (2007) 736-746.